

Three-dimensionally branched carbon nanowebs as air-cathode for redox-mediated Li-O₂ batteries



Hee-Dae Lim ^{a,1}, Young Soo Yun ^{b,1}, Youngmin Ko ^a, Youngjoon Bae ^a, Min Yeong Song ^c, Hyeon Ji Yoon ^c, Kisuk Kang ^{a, d, **, 1}, Hyoung-Joon Jin ^{c, *, 1}

^a Department of Materials Science and Engineering, Seoul National University, 1 Gwanak-ro, Gwanak-gu, Seoul 151-742, Republic of Korea

^b Department of Chemical Engineering, Kangwon National University, Samcheok 245-711, Republic of Korea

^c Department of Polymer Science and Engineering, Inha University, Incheon 402-751, Republic of Korea

^d Center for Nanoparticle Research, Institute for Basic Science (IBS), Seoul National University, 1 Gwanak-ro, Gwanak-gu, Seoul 151-742, Republic of Korea

ARTICLE INFO

Article history:

Received 12 January 2017

Received in revised form

8 March 2017

Accepted 10 March 2017

Available online 13 March 2017

Keywords:

Carbon nanoweb

Macroporous carbon

Carbon nanofiber

Electrode

Li-O₂ batteries

Li₂O₂

ABSTRACT

The optimal design of air-electrodes is one of the important keys to achieve the high rechargeability of Li-O₂ batteries, however, remains as challenging issue to date. Herein, we propose an air-electrode architecture based on three-dimensionally open macroporous carbon nanowebs (3-DOM-CNWs), which can be easily scaled-up maintaining its hierarchical structure of nano/micrometer-scale pores. It is demonstrated that the open macroporous nanoweb electrode is particularly advantageous for Li-O₂ batteries utilizing the redox mediators in the electrolyte by facilitating the efficient transport of them. The 3-DOM-CNWs electrode could deliver higher specific capacity (~14,000 mAh g⁻¹) and longer cyclic stability with a better energy efficiency than the conventionally used Ketjen black (KB)-based electrode for redox-mediated Li-O₂ batteries, while the specific surface area of 3-DOM-CNWs is only one fourteenth of that of the KB-based air-electrode. This result clearly demonstrates that the electrode architecture based on the hierarchical pore structures significantly enhances the electrochemical performance of Li-O₂ batteries by aiding in the transport not only of lithium and oxygen but also the redox mediators.

© 2017 Elsevier Ltd. All rights reserved.

1. Introduction

Li-O₂ batteries have been proposed as a next-generation power option for large-scale energy storage devices such as electric vehicles, as they are capable of delivering a high energy density (~3200 Wh kg⁻¹), which surpasses that of conventional Li-ion batteries [1–4]. The electrochemical reaction in Li-O₂ batteries is based on the formation of solid discharge products, *i.e.*, lithium peroxide (Li₂O₂), on the surface of conductive air-electrodes according to the following reaction: 2Li⁺ + O₂ + 2e⁻ → Li₂O₂ (2.96 V vs. Li/Li⁺) [5–8]. The Li₂O₂ particles are electrochemically grown upon discharge with various morphologies and particle sizes from a few to hundreds of nanometers depending on the operation

condition [9–11]. In conventional Li-O₂ batteries, carbon blacks (CBs) with high active surface areas have been used as electrode materials, since they can accommodate a large amount of Li₂O₂ on their surface and inner pores during discharge [12–14]. However, CB-based air cells have suffered from a poor cyclic performance and a low energy efficiency due to the premature clogging of the air-electrode by the discharge products, which, thereby, block the oxygen and Li diffusion channels [15,16]. Accordingly, considerable efforts have been focused on designing electrode architectures to achieve a reversible formation and decomposition of Li₂O₂ [17–22]. However, although many carbon-based electrodes have been suggested, the clogging phenomenon on carbon surfaces remains a crucial issue that deteriorates the cyclic performance of Li-O₂ batteries. Moreover, with the recent introduction of the soluble catalysts, which should effectively shuttle within the air-electrode to decompose the discharge products, the electrode architecture becomes more critical [23–28].

Recently, it was revealed that the nature of the discharge products can significantly vary by the properties of the electrolyte, where large toroidal Li₂O₂ products are prone to form via the

* Corresponding author. Department of Polymer Science and Engineering, Inha University, Incheon 402-751, Republic of Korea.

** Corresponding author. Department of Materials Science and Engineering, Seoul National University, 1 Gwanak-ro, Gwanak-gu, Seoul 151-742, Republic of Korea.

E-mail addresses: matlgen1@snu.ac.kr (K. Kang), hjin@inha.ac.kr (H.-J. Jin).

¹ These authors contributed equally to this work.

solution-mediated process in the electrolyte with the high solvating effect, on the other hand, film-like Li_2O_2 formation occurs in the low donor number electrolyte [5,29]. As the solution-mediated process leads to the formation of large-size Li_2O_2 , the specific capacity is generally improved by the use of such electrolytes, thus recent studies attempted to further exploit the solution-mediated process by altering the components or operating conditions of $\text{Li}-\text{O}_2$ batteries [6,30,31]. In this case, the issue of clogging the electrode, which have been commonly observed for the film-type discharge products in most of $\text{Li}-\text{O}_2$ batteries becomes less serious, instead, considering that the bulk toroidal Li_2O_2 mainly grows first in the electrolyte and then deposits on the electrode surface, a large, open, macroporous electrode structure with well-developed conducting networks is required in order to efficiently accommodate the large toroidal Li_2O_2 particles. Furthermore, since the large toroidal discharge product inevitably requires the soluble catalysts, the electrode architecture considering the transport of redox mediator would become of critical in the performance of $\text{Li}-\text{O}_2$ batteries.

Herein, we report three-dimensionally open macroporous carbon nanowebs (3-DOM-CNWs) composed of entangled carbon nanofibers, as an air-electrode platform for redox-mediated $\text{Li}-\text{O}_2$ batteries. The electrode performance is demonstrated in a $\text{Li}-\text{O}_2$ cell employing the LiNO_3 dissolved in dimethylacetamide (DMA), wherein the LiNO_3 salt works as a liquid-type redox catalyst ($\text{NO}_2^-/\text{NO}_2$) in the hydrophilic DMA, facilitating the Li_2O_2 decomposition during charge [32–35]. The multi-dimensionally branched macroporous structure composed of high aspect ratio carbon components displays a more stable cyclability and better energy efficiency than the conventional CB-based air-electrode, demonstrating that the electrode architecture plays a central role for the electrochemical performances of redox-mediated $\text{Li}-\text{O}_2$ batteries.

2. Experimental

2.1. Preparation of 3-DOM-CNWs

Bacterial cellulose (BC) hydrogels were synthesized using *Aacetobacter xylinum* BRC 5 in the Hestrin and Schramm (HS) medium according to a previously reported method [36]. The BC hydrogels were immersed in tert-butanol to exchange the solvents. After freezing at -30°C for 6 h, the BCs were freeze-dried at -45°C and 4.5 Pa for 72 h. The as-prepared BC cryogels were heated to 800°C for 2 h under a N_2 atmosphere. A heating rate of 2°C min^{-1} and a N_2 flow rate of 200 ml min^{-1} were applied during the pyrolysis process. The resulting 3-DOM-CNWs were stored in a vacuum oven at 30°C .

2.2. Electrochemical test and analysis

The air-electrode was composed of a mixture of carbon and binder at a ratio of 8:2, which was coated onto the current collector (Ni mesh). The as-prepared electrode, separator (Whatman GF/D), and Li metal were assembled into a Swagelok-type cell. The electrode and separator were soaked in electrolyte (1 M LiNO_3 in DMA) for 10 min prior to use. All the cells were tested using a potentiogalvanostat (WBCS 3000, WonATech, Korea) in a pure oxygen atmosphere at 770 Torr. In addition, X-ray photoelectron spectroscopy (XPS, PHI 5700 ESCA, USA), X-ray diffractometry (XRD, Rigaku, D/MAX-RB diffractometer, Tokyo, Japan), field-emission scanning electron microscopy (FE-SEM, Philips, XL 30 FEG, Eindhoven, Netherlands), and field-emission transmission electron microscopy (FE-TEM, JEM2100F, JEOL, Japan) were used to characterize the electrodes. In addition, the pore structures of the samples were analyzed using nitrogen adsorption and desorption isotherms

recorded by a surface area and porosimetry analyzer (Tristar, Micromeritics, USA) at -196°C .

3. Results and discussion

The morphology of the 3-DOM-CNWs was characterized by FE-SEM and FE-TEM images, as shown in Fig. 1(a)–1(c). The 3-DOM-CNWs are composed of numerous, loosely entangled carbon nanofibers with diameters of $\sim 50 \text{ nm}$ and well-developed large open spaces corresponding to macropores. This unique pore structure originates from a microbe-derived nanostructure that is well-maintained during the pyrolysis process [Fig. S1]. Note that the carbon nanofibers are multi-dimensionally interconnected to each other, which can provide electrical conducting pathways even when their surface is entirely covered by discharge products and/or byproducts in the course of discharge of $\text{Li}-\text{O}_2$ batteries. A high-resolution FE-TEM image shows no long-range carbon ordering, indicating that 3-DOM-CNWs have an amorphous carbon structure [Fig. 1(c)]. The microstructure was investigated in further detail by Raman spectroscopy and XRD, as shown in Fig. 1(d) and (e), respectively. The Raman spectrum of 3-DOM-CNWs shows distinct *D* and *G* bands centered at 1345 and 1590 cm^{-1} , respectively [Fig. 1(d)], corresponding to the disordered A_{1g} breathing mode of the six-member aromatic ring close to the basal edge and the hexagonal carbon structure related to the E_{2g} vibration mode of the sp^2 -hybridized C atoms, respectively. The intensity ratio of the *D* and *G* bands (I_D/I_G) for 3-DOM-CNWs was ~ 0.98 , indicating that they consist of nanometer-sized hexagonal carbon layers. In addition, the XRD pattern of 3-DOM-CNWs shows a broad graphite (002) peak [Fig. 1(e)], indicating that the stacking ordering of their hexagonal carbon structures is poor.

The surface properties of the 3-DOM-CNWs were investigated by XPS, as shown in Fig. 1(f) and (g). In the C 1s XPS spectrum, C-O bonding and C=O bonding peaks were observed centered at 285.4 and 289.4 eV , respectively, including a main C-C bonding peak centered at 284.4 eV [Fig. 1(f)]. In the O 1s XPS spectrum, two distinct peaks representing the C=O bonding and C-O bonding were centered at 531.8 and 533.2 eV , respectively [Fig. 1(g)]. The C/O ratio was approximately 20.2. These small amount of oxygen functional groups could be introduced onto edge sites of the hexagonal carbon structures during the pyrolysis process, which may enhance the wettability of the hydrophobic carbon-based electrode in a hydrophilic electrolyte. Furthermore, the pore structure of 3-DOM-CNWs was characterized by a nitrogen adsorption/desorption isotherm test, as shown in Fig. 1(h) and its inset. The isotherm curve shape is close to an IUPAC type-II isotherm, indicative of a macroporous structure. However, the isotherm curve also shows some monolayer adsorption of nitrogen gas in the low relative pressure (<0.1) section, which means that 3-DOM-CNWs also contain micropores. These small pores could originate from a random aggregation of hexagonal carbon basic structural units (BSUs). The pore volume as a function of the pore width is depicted in the inset of Fig. 1(h), which shows that a broad range of pore widths are present in the 3-DOM-CNWs. The specific surface area of the 3-DOM-CNWs is $100.7 \text{ m}^2 \text{ g}^{-1}$, of which micropores and mesopores were $23.3 \text{ m}^2 \text{ g}^{-1}$ and $77.4 \text{ m}^2 \text{ g}^{-1}$, respectively.

The fabricated 3-DOM-CNW was employed as an air-electrode in a $\text{Li}-\text{O}_2$ cell using 1 M LiNO_3 in DMA, and its electrochemical performance was compared with a Ketjen black (KB) electrode, as shown in Fig. 2. KB has been widely used for $\text{Li}-\text{O}_2$ batteries due to its high surface area and good electrical conductivity [12,13], and these properties are confirmed in Fig. S2. Although the specific surface area of the 3-DOM-CNWs is ~ 14 times lower ($100.7 \text{ m}^2 \text{ g}^{-1}$) than that of KBs ($\sim 1400 \text{ m}^2 \text{ g}^{-1}$), it is noted that the 3-DOM-CNW electrode shows a much enhanced discharge capacity of

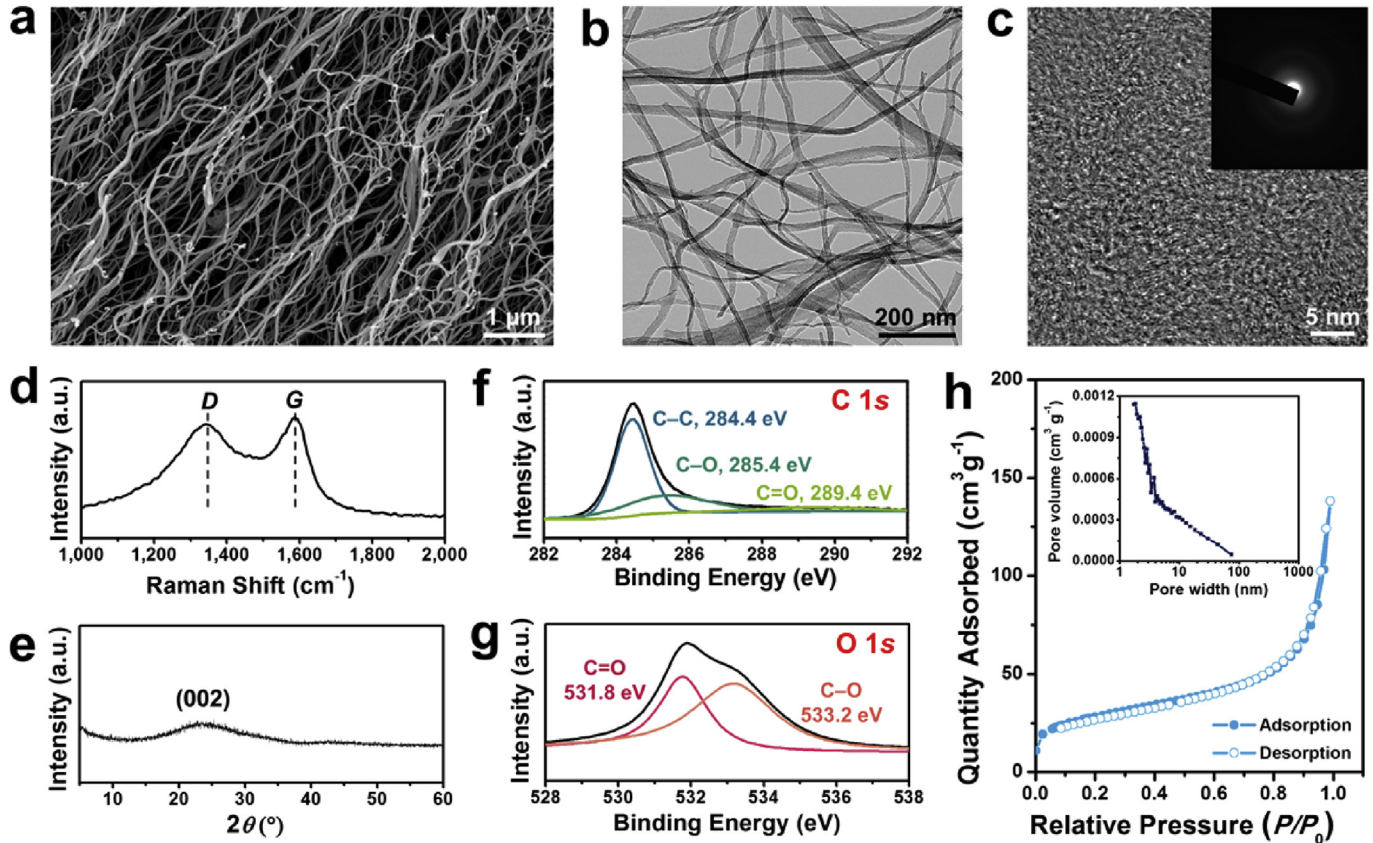


Fig. 1. Characteristics of the 3-DOM-CNWs. (a) FE-SEM and (b), (c) FE-TEM images with different magnifications. The inset of Fig. 1(c) shows the selected area diffraction pattern. (d) Raman spectrum and (e) XRD pattern. XPS (f) C 1s and (g) O 1s spectra. (h) Nitrogen adsorption and desorption isotherm curves. Inset: pore size distribution. (A colour version of this figure can be viewed online.)

~14,000 mAh g⁻¹, which is a higher value than that (~8000 mAh g⁻¹) of the KB electrode [Fig. 2(a)]. The results contradict a general belief that a carbon electrode with a high specific surface area yields a high discharge capacity. The discharge products were characterized by XRD, as shown in Fig. 2(b). The major discharge products in both 3-DOM-CNW- and KB-based electrodes are Li₂O₂, which agrees well with previous reports [32,34], wherein the LiNO₃/DMA electrolyte was used. The morphologies of the discharge products were observed using FE-SEM, as shown in Fig. 2(c) and (d). After discharge, both electrodes were carefully washed with the DMA electrolyte and then dried in a vacuum oven for *ex situ* characterization, which was carried without exposing the samples to air. For the KB electrode, toroidal particles with diameters between ~100 and ~400 nm were mainly found on the surface of the KB electrode after discharge [Fig. 2(c)]. This confirms that the small pores of the KB particles do not contribute to accommodating the large toroidal Li₂O₂ particles. In contrast, numerous toroidal Li₂O₂ particles are entangled within the carbon nanofiber branches of the 3-DOM-CNWs and/or are well deposited in the inner spaces of the electrode [Fig. 2(d)]. Magnified images are provided in Fig. S3. Additionally, the morphologies of both KB and 3-DOM-CNW electrodes were observed after a deep discharge, as shown in Fig. 3. The discharge products are densely deposited on the surface of KB electrode, which appears to have no conducting pathways for either electrons or Li ions [Fig. 3(a) and (b)]. On the other hand, 3-DOM-CNW electrodes still exhibit open spaces, and the toroidal Li₂O₂ particles are bound by carbon nanofibers, indicating the presence of both electrically conductive networks and Li-ion diffusion pathways [Fig. 3(c) and (d)]. These *ex situ* FE-SEM

results evidently demonstrate that the open macroporous and interconnected electrode structure can more efficiently store large Li₂O₂ particles, highlighting the merits of 3-DOM-CNWs electrode.

The cyclability of the 3-DOM-CNW electrode was compared to that of the KB electrode, as shown in Fig. 4(a) and (b). For both electrodes, the discharge voltages are nearly identical exhibiting a potential plateau around 2.8 V during consecutive cycles; however, their charge properties are notably different. While the charge voltages of the KB electrode gradually increased as the cycling proceeded, both the discharge and charge profiles of the 3-DOM-CNW electrode remained stable and reversible. The charge process of redox-mediated Li-O₂ batteries using the LiNO₃/DMA electrolyte mainly proceeds by the redox reaction of NO₂⁻/NO₂ [33,34]. During the charge, the NO₂⁻ is first oxidized to NO₂ prior to the electrochemical decomposition of Li₂O₂, and then, the oxidized NO₂ chemically reacts with Li₂O₂, decomposing into Li ions and O₂. NO₂ plays a role of a redox mediator in this electrolyte-catalytic system, thus making the system as a redox-mediated Li-O₂ battery. In this case, the charge efficiency can be affected by how easily NO₂⁻/NO₂ ions can transport within the air-electrode to decompose Li₂O₂ during charge. Considering that the hierarchically macroporous structure facilitates the mass transfer of ions in the electrolyte, 3-DOM-CNW electrodes could facilitate the rapid diffusion of the liquid catalyst. Also, it was reported that a structural design of porous carbon networks can guarantee a fast ion transfer and improve kinetic performance of lithium batteries [37]. Accordingly, the NO₂⁻/NO₂ ions that could freely diffuse in the 3-DOM-CNW electrode could effectively decompose Li₂O₂ during charge, constantly maintaining the charging potential around 3.6 V during

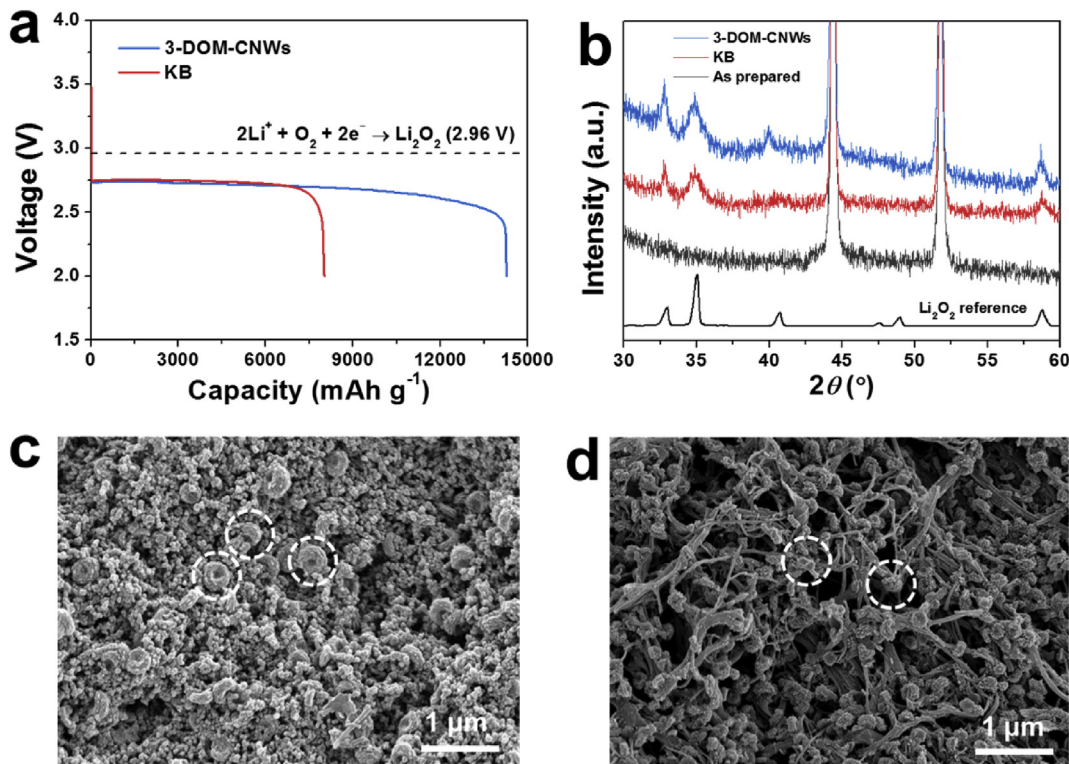


Fig. 2. (a) Discharge profile of Li-O₂ cells at a constant current of 300 mA g⁻¹ to a 2.0 V cut-off. (b) XRD results of the air electrodes based on 3-DOM-CNWs and KB after full discharge. Peaks are normalized to the Ni current collector around 44.4° and 51.8°. FE-SEM images of (c) the KB electrode and (d) the 3-DOM-CNW electrode after discharge to 500 mAh g⁻¹. (A colour version of this figure can be viewed online.)

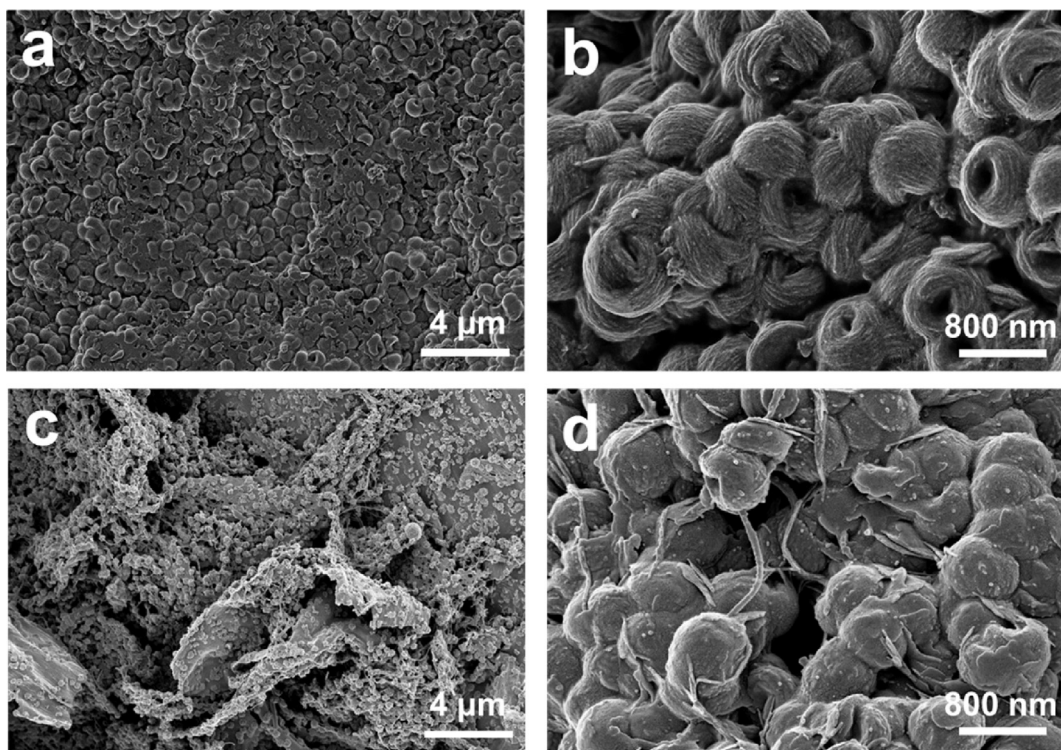


Fig. 3. FE-SEM images of (a,b) the KB electrode and (c,d) the 3-DOM-CNW electrode after full discharge to 2.0 V. The capacities of the KB and 3-DOM-CNW electrodes are approximately 8000 and 14,000 mAh g⁻¹, respectively.

cycles. In contrast, the small pores of the KB electrode could be relatively unfavorable for the diffusion of the liquid catalyst, and

the Li₂O₂ deposited mainly on the surface of the KB electrode can also hinder the NO₂/NO redox activity, which leads to a low charge

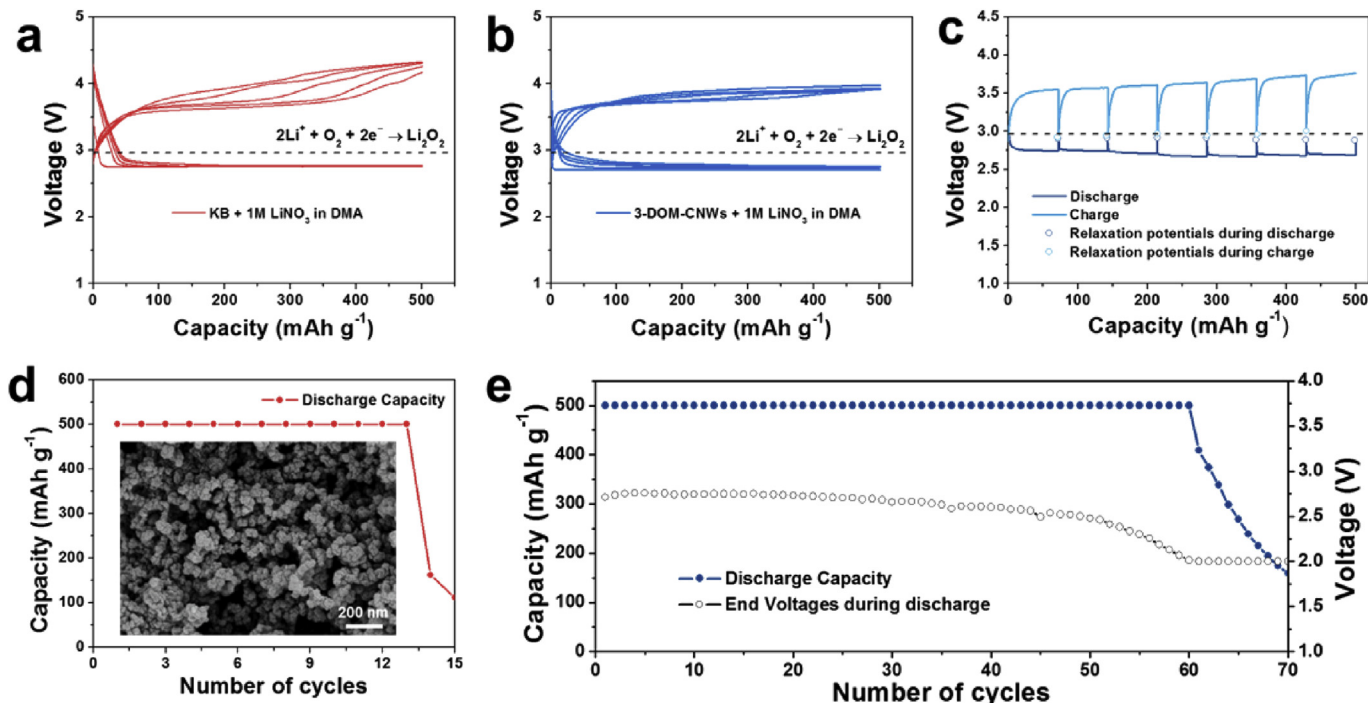


Fig. 4. Electrochemical profiles of the Li-O₂ cells using (a) the KB electrode and (b) the 3-DOM-CNPs electrode at a constant current of 300 mA g⁻¹ with the capacity limited to 500 mAh g⁻¹. (c) GITT measurement of the 3-DOM-CNPs electrode for the first cycle. The dotted line indicates the theoretical formation voltage of Li₂O₂ (2.96 V), and the cell is fully relaxed for 10 h at each point. Cyclability of the cells using (d) the KB electrode (inset: FE-SEM image showing the morphology of the KB carbon) and (e) the 3-DOM-CNPs electrode. (A colour version of this figure can be viewed online.)

efficiency and gradual increase in the charge polarization, as shown in Fig. 4(a). The limited activity of the soluble catalyst in the KB electrode was also demonstrated in the previous report [23]. To probe the formation and decomposition of Li₂O₂ in 3-DOM-CNPs electrode in further detail, GITT measurement was conducted, as shown in Fig. 4(c). The GITT profile and relaxation potentials at each point are indicated by blue lines and circles, respectively. As shown in Fig. 4(c), each relaxation potential is close to the theoretical formation voltage of Li₂O₂ (2.96 V), implying that the discharge and charge processes are reversible. The effects of the structural differences in the air-electrodes are clearly confirmed by the cyclability comparison between the KB and 3-DOM-CNPs electrodes in Fig. 4(d) and (e). While the KB electrode quickly loses the reversibility after only 13 cycles with a limited capacity of 500 mAh g⁻¹, the 3-DOM-CNPs electrode shows an enhanced cyclability over 60 cycles. These results indicate that the 3-DOM-CNPs electrode is capable of offering the enhanced reversible capacity and charge efficiency in redox-mediated Li-O₂ batteries.

4. Conclusion

In summary, 3-DOM-CNPs were fabricated from BC cryogels by simple pyrolysis for use as the air-electrode in the redox-mediated Li-O₂ batteries. The 3-DOM-CNPs exhibited the open macrostructure composed of interconnected carbon nanofibers, which could efficiently store large toroidal Li₂O₂ products in the overall internal space. The macroporous structure was beneficial not only with respect to effectively accommodating the large discharge products from the solution-mediated discharge process but also offering more facile transport for the redox mediators that could enhance the rechargeability of the Li-O₂ cell. As a result, the cell employing 3-DOM-CNPs could deliver a more stable cyclability of over ~60 cycles with a better charge efficiency and the twice higher

specific capacity than those of the KB electrode (~13 cycles) in spite of the much smaller surface area of 3-DOM-CNPs (one fourteenth of KB). Our findings on the air-electrode design imply that the discharge capacity of Li-O₂ cells based on the solution mediated process is less dependent on the specific surface area of the active electrode, but is greatly affected by the pore structure. Furthermore, for Li-O₂ cells employing the redox mediators, the electrode architecture should be carefully thought out considering the transport issues of the redox mediators, which can significantly influence on the charging efficiency and cycling stability.

Acknowledgements

This work was supported by the National Research Foundation of Korea (NRF) grand funded by the Korea government (MSIP) (No. 2015R1A2A1A10055991) and also supported by Basic Science Research Program through the National Research Foundation of Korea (NRF) funded by the Ministry of Education (NRF-2016R1A2B4009601). This work was supported by the HMC (Hyundai Motor Company).

Appendix A. Supplementary data

Supplementary data related to this article can be found at <http://dx.doi.org/10.1016/j.carbon.2017.03.033>.

References

- [1] P.G. Bruce, S.A. Freunberger, L.J. Hardwick, J.-M. Tarascon, Li-O₂ and Li-S batteries with high energy storage, *Nat. Mater.* 11 (2012) 19–29.
- [2] F. Cheng, J. Chen, Metal-air batteries: from oxygen reduction electrochemistry to cathode catalysts, *Chem. Soc. Rev.* 41 (2012) 2172–2192.
- [3] T. Liu, M. Leskes, W. Yu, A.J. Moore, L. Zhou, P.M. Bayley, G. Kim, C.P. Grey, Cycling Li-O₂ batteries via LiOH formation and decomposition, *Science* 350 (2015) 530–533.

- [4] H.-D. Lim, B. Lee, Y. Zheng, J. Hong, J. Kim, H. Gwon, Y. Ko, M. Lee, K. Cho, K. Kang, Rational design of redox mediators for advanced Li–O₂ batteries, *Nat. Energy* 1 (2016) 16066.
- [5] N.B. Aetukuri, B.D. McCloskey, J.M. García, L.E. Krupp, V. Viswanathan, A.C. Luntz, Solvating additives drive solution-mediated electrochemistry and enhance toroid growth in non-aqueous Li–O₂ batteries, *Nat. Chem.* 7 (2015) 50–56.
- [6] X. Gao, Y. Chen, L. Johnson, P.G. Bruce, Promoting solution phase discharge in Li–O₂ batteries containing weakly solvating electrolyte solutions, *Nat. Mater.* 15 (2016) 882–888.
- [7] E. Yilmaz, C. Yogi, K. Yamanaka, T. Ohta, H.R. Byon, Promoting formation of noncrystalline Li₂O₂ in the Li–O₂ battery with RuO₂ nanoparticles, *Nano Lett.* 13 (2013) 4679–4684.
- [8] X. Zhang, X.-G. Wang, Z. Xie, Z. Zhou, Recent progress in rechargeable alkali metal–air batteries, *Green Energy Environ.* 1 (2016) 4–17.
- [9] C. Laoire, S. Mukerjee, E.J. Plichta, M.A. Hendrickson, K.M. Abraham, Rechargeable lithium/TEGDME–LiPF₆/O₂ battery, *J. Electrochem. Soc.* 158 (2011) A302–A308.
- [10] D. Xu, Z.-I Wang, J.-j Xu, Li Zhang, X.-b Zhang, Novel DMSO–based electrolyte for high performance rechargeable Li–O₂ batteries, *Chem. Commun.* 48 (2012) 6948–6950.
- [11] B.M. Gallant, R.R. Mitchell, D.G. Kwabi, J. Zhou, L. Zuin, C.V. Thompson, Y. Shao–Horn, Chemical and morphological changes of Li–O₂ battery electrodes upon cycling, *J. Phys. Chem. C* 116 (2012) 20800–20805.
- [12] J. Xiao, D. Wang, W. Xu, D. Wang, R.E. Williford, J. Liu, J.-G. Zhang, Optimization of air electrode for Li/Air batteries, *J. Electrochem. Soc.* 157 (2010) A487–A492.
- [13] S.D. Beattie, D.M. Manolescu, S.L. Blair, High–capacity lithium–air cathodes, *J. Electrochem. Soc.* 156 (2009) A44–A47.
- [14] T. Ogasawara, A. Débart, M. Holzapfel, P. Novák, P.G. Bruce, Rechargeable Li₂O₂ electrode for lithium batteries, *J. Am. Chem. Soc.* 128 (2006) 1390–1393.
- [15] C. Xia, M. Waletzko, L. Chen, K. Peppier, P.J. Klar, Janek Jr., Evolution of Li₂O₂ growth and its effect on kinetics of Li–O₂ batteries, *ACS Appl. Mater. Interfaces* 6 (2014) 12083–12092.
- [16] J. Read, Characterization of the lithium/oxygen organic electrolyte battery, *J. Electrochem. Soc.* 149 (2002) A1190–A1195.
- [17] W.-H. Ryu, F.S. Gittleson, M. Schwab, T. Goh, A.D. Taylor, A mesoporous catalytic membrane architecture for lithium–oxygen battery systems, *Nano Lett.* 15 (2014) 434–441.
- [18] H.-D. Lim, K.-Y. Park, H. Song, E.Y. Jang, H. Gwon, J. Kim, Y.H. Kim, M.D. Lima, R.O. Robles, X. Lepro, R.H. Baughman, K. Kang, Enhanced power and rechargeability of a Li–O₂ battery based on a hierarchical–fibril CNT electrode, *Adv. Mater.* 25 (2013) 1348–1352.
- [19] H. Kim, H.-D. Lim, J. Kim, K. Kang, Graphene for advanced Li/S and Li/air batteries, *J. Mater. Chem. A* 2 (2013) 33–47.
- [20] Z. Guo, D. Zhou, X. Dong, Z. Qiu, Y. Wang, Y. Xia, Ordered hierarchical mesoporous/macroporous carbon: a high-performance catalyst for rechargeable Li–O₂ batteries, *Adv. Mater.* 25 (2013) 5668–5672.
- [21] F. Li, Y. Chen, D.-M. Tang, Z. Jian, C. Liu, D. Golberg, A. Yamada, H. Zhou, Performance-improved Li–O₂ battery with Ru nanoparticles supported on binder-free multi-walled carbon nanotube paper as cathode, *Energy Environ. Sci.* 7 (2014) 1648–1652.
- [22] X. Lin, L. Zhou, T. Huang, A. Yu, Hierarchically porous honeycomb-like carbon as a lithium–oxygen electrode, *J. Mater. Chem. A* 1 (2013) 1239–1245.
- [23] H.-D. Lim, H. Song, J. Kim, H. Gwon, Y. Bae, K.-Y. Park, J. Hong, H. Kim, T. Kim, Y.H. Kim, X. Lepro, R. Ovalle-Robles, R.H. Baughman, K. Kang, Superior rechargeability and efficiency of lithium–oxygen batteries: hierarchical air electrode architecture combined with a soluble catalyst, *Angew. Chem. Int. Ed.* 53 (2014) 3926–3931.
- [24] Y. Chen, S.A. Freunberger, Z. Peng, O. Fontaine, P.G. Bruce, Charging a Li–O₂ battery using a redox mediator, *Nat. Chem.* 5 (2013) 489–494.
- [25] D. Kundu, R. Black, B. Adams, L.F. Nazar, A highly active low voltage redox mediator for enhanced rechargeability of lithium–oxygen batteries, *ACS Central Sci.* 1 (2015) 510–515.
- [26] W.-H. Ryu, F.S. Gittleson, J.M. Thomsen, J. Li, M.J. Schwab, G.W. Brudvig, A.D. Taylor, Heme biomolecule as redox mediator and oxygen shuttle for efficient charging of lithium–oxygen batteries, *Nat. Commun.* 7 (2016) 12925.
- [27] F. Li, T. Zhang, H. Zhou, Challenges of non-aqueous Li–O₂ batteries: electrolytes, catalysts, and anodes, *Energy Environ. Sci.* 6 (2013) 1125–1141.
- [28] Z. Zhang, J. Bao, C. He, Y. Chen, J. Wei, Z. Zhou, Hierarchical carbon–nitrogen architectures with both mesopores and macrochannels as excellent cathodes for rechargeable Li–O₂ batteries, *Adv. Funct. Mater.* 24 (2014) 6826–6833.
- [29] D. Aurbach, B.D. McCloskey, L.F. Nazar, P.G. Bruce, Advances in understanding mechanisms underpinning lithium–air batteries, *Nat. Energy* 1 (2016) 16128.
- [30] C.M. Burke, V. Pande, A. Khetan, V. Viswanathan, B.D. McCloskey, Enhancing electrochemical intermediate solvation through electrolyte anion selection to increase nonaqueous Li–O₂ battery capacity, *Proc. Natl. Acad. Sci.* 112 (2015) 9293–9298.
- [31] L. Johnson, C. Li, Z. Liu, Y. Chen, S.A. Freunberger, P.C. Ashok, B.B. Praveen, K. Dholakia, J.-M. Tarascon, P.G. Bruce, The role of Li₂O₂ solubility in O₂ reduction in aprotic solvents and its consequences for Li–O₂ batteries, *Nat. Chem.* 6 (2014) 1091–1099.
- [32] W. Walker, V. Giordani, J. Uddin, V.S. Bryantsev, G.V. Chase, D. Addison, A Rechargeable Li–O₂ battery using a lithium nitrate/N,N-Dimethylacetamide electrolyte, *J. Am. Chem. Soc.* 135 (2013) 2076–2079.
- [33] J. Uddin, V.S. Bryantsev, V. Giordani, W. Walker, G.V. Chase, D. Addison, Lithium nitrate as regenerable SEI stabilizing agent for rechargeable Li/O₂ batteries, *J. Phys. Chem. Lett.* 4 (2013) 3760–3765.
- [34] D. Sharon, D. Hirsberg, M. Afri, A. Garsuch, A.A. Frimer, D. Aurbach, Reactivity of amide based solutions in lithium–oxygen cells, *J. Phys. Chem. C* 118 (2014) 15207–15213.
- [35] D. Sharon, D. Hirsberg, M. Afri, F. Chesneau, R. Lavi, A.A. Frimer, Y.-K. Sun, D. Aurbach, Catalytic behavior of lithium nitrate in Li–O₂ cells, *ACS Appl. Mater. Interfaces* 7 (2015) 16590–16600.
- [36] Y.S. Yun, H. Bak, H.-J. Jin, Porous carbon nanotube electrodes supported by natural polymeric membranes for PEMFC, *Synth. Met.* 160 (2010) 561–565.
- [37] S. Xin, Y.G. Guo, L.-J. Wan, Nanocarbon networks for advanced rechargeable lithium batteries, *Acc. Chem. Res.* 45 (2012) 1759–1769.